ERRATUM: "MOA-2008-BLG-379Lb: A MASSIVE PLANET FROM A HIGH MAGNIFICATION EVENT WITH A FAINT SOURCE" (2014, ApJ, 780, 123)

D. Suzuki[1,16], A. Udalski[2,17], T. Sumi[1,16], D. P. Bennett[3,16], I. A. Bond[4,16],

AND

F. Abe[5], C. S. Botzler[6], M. Freeman[6], M. Fukagawa[1], A. Fukui[7], K. Furusawa[5], Y. Itow[5], C. H. Ling[4], K. Masuda[5], Y. Matsubara[5], Y. Muraki[8], K. Ohnishi[9], N. Rattenbury[6], To. Saito[10], H. Shibai[1], D. J. Sullivan[11], K. Suzuki[5], W. L. Sweatman[4], S. Takino[3], P. J. Tristram[12], K. Wada[1], P. C. M. Yock[6]

(MOA COLLABORATION),

M. K. Szymański[2], M. Kubiak[2], I. Soszyński[2], G. Pietrzyński[2,13], R. Poleski[2,14], K. Ulaczyk[2], AND Ł. Wyrzykowski[2,15]

(OGLE COLLABORATION)

[1] Department of Earth and Space Science, Graduate School of Science, Osaka University, 1-1 Machikaneyama, Toyonaka, Osaka 560-0043, Japan
[2] Warsaw University Observatory, Al. Ujazdowskie 4, 00-478 Warszawa, Poland
[3] Department of Physics, University of Notre Dame, Notre Dame, IN 46556, USA
[4] Institute of Information and Mathematical Sciences, Massey University, Private Bag 102-904, North Shore Mail Centre, Auckland, New Zealand
[5] Solar–Terrestrial Environment Laboratory, Nagoya University, Furo-cho, Chikusa, Nagoya, Aichi 464-8601, Japan
[6] Department of Physics, University of Auckland, Private Bag 92019, Auckland, New Zealand
[7] Okayama Astrophysical Observatory, National Astronomical Observatory, 3037-5 Honjo, Kamogata, Asakuchi, Okayama 719-0232, Japan
[8] Department of Physics, Konan University, Nishiokamoto 8-9-1, Kobe 658-8501, Japan
[9] Nagano National College of Technology, Nagano 381-8550, Japan
[10] Tokyo Metropolitan College of Industrial Technology, Tokyo 116-8523, Japan
[11] School of Chemical and Physical Sciences, Victoria University, Wellington, New Zealand
[12] Mt. John University Observatory, University of Canterbury, P.O. Box 56, Lake Tekapo 8770, New Zealand
[13] Departamento de Astronomia, Universidad de Concepción, Casilla 160-C, Concepción, Chile
[14] Department of Astronomy, The Ohio State University, 140 West 18th Avenue, Columbus, OH 43210, USA
[15] Institute of Astronomy, University of Cambridge, Madingley Road, Cambridge CB3 0HA, UK
Received 2014 May 6; published 2014 May 27

Due to an error at the publisher, the incorrect physical parameters of the lens system MOA-2008-BLG-379 were given in the Abstract of the published paper. The corrected Abstract appears below. IOP Publishing sincerely regrets this error.

We report on the analysis of the high microlensing event MOA-2008-BLG-379, which has a strong microlensing anomaly at its peak due to a massive planet with a mass ratio of $q = 6.9 \times 10^{-3}$. Because the faint source star crosses the large resonant caustic, the planetary signal dominates the light curve. This is unusual for planetary microlensing events, and as a result, the planetary nature of this light curve was not immediately noticed. The planetary nature of the event was found when the Microlensing Observations in Astrophysics (MOA) Collaboration conducted a systematic study of binary microlensing events previously identified by the MOA alert system. We have conducted a Bayesian analysis based on a standard Galactic model to estimate the physical parameters of the lens system. This yields a host star mass of $M_{\rm L} = 0.56^{+0.24}_{-0.27} \, M_\odot$ orbited by a planet of mass $m_{\rm P} = 4.1^{+1.7}_{-1.9} \, M_{\rm Jup}$ at an orbital separation of $a = 3.3^{+1.7}_{-1.2}$ AU at a distance of $D_{\rm L} = 3.3^{+1.3}_{-1.2}$ kpc. The faint source magnitude of $I_{\rm S} = 21.30$ and relatively high lens–source relative proper motion of $\mu_{\rm rel} = 7.6 \pm 1.6$ mas yr^{-1} imply that high angular resolution adaptive optics or *Hubble Space Telescope* observations are likely to be able to detect the source star, which would determine the masses and distance of the planet and its host star.

---

[16] Microlensing Observations in Astrophysics (MOA) Collaboration.
[17] Optical Gravitational Lensing Experiment (OGLE) Collaboration.

MOA-2008-BLG-379Lb: A MASSIVE PLANET FROM A HIGH MAGNIFICATION EVENT WITH A FAINT SOURCE

D. SUZUKI[1,16], A. UDALSKI[2,17], T. SUMI[1,16], D. P. BENNETT[3,16], I. A. BOND[4,16],

AND

F. ABE[5], C. S. BOTZLER[6], M. FREEMAN[6], M. FUKAGAWA[1], A. FUKUI[7], K. FURUSAWA[5], Y. ITOW[5], C. H. LING[4], K. MASUDA[5],
Y. MATSUBARA[5], Y. MURAKI[8], K. OHNISHI[9], N. RATTENBURY[6], TO. SAITO[10], H. SHIBAI[1], D. J. SULLIVAN[11], K. SUZUKI[5],
W. L. SWEATMAN[4], S. TAKINO[3], P. J. TRISTRAM[12], K. WADA[1], AND P. C. M. YOCK[6]
(MOA COLLABORATION)
M. K. SZYMAŃSKI[2], M. KUBIAK[2], I. SOSZYŃSKI[2], G. PIETRZYŃSKI[2,13], R. POLESKI[2,15], K. ULACZYK[2], AND Ł. WYRZYKOWSKI[2,14]
(OGLE COLLABORATION)

[1] Department of Earth and Space Science, Graduate School of Science, Osaka University, 1-1 Machikaneyama, Toyonaka, Osaka 560-0043, Japan
[2] Warsaw University Observatory, Al. Ujazdowskie 4, 00-478 Warszawa, Poland
[3] Department of Physics, University of Notre Dame, Notre Dame, IN 46556, USA
[4] Institute of Information and Mathematical Sciences, Massey University, Private Bag 102-904, North Shore Mail Centre, Auckland, New Zealand
[5] Solar-Terrestrial Environment Laboratory, Nagoya University, Furo-cho, Chikusa, Nagoya, Aichi 464-8601, Japan
[6] Department of Physics, University of Auckland, Private Bag 92019, Auckland, New Zealand
[7] Okayama Astrophysical Observatory, National Astronomical Observatory, 3037-5 Honjo, Kamogata, Asakuchi, Okayama 719-0232, Japan
[8] Department of Physics, Konan University, Nishiokamoto 8-9-1, Kobe 658-8501, Japan
[9] Nagano National College of Technology, Nagano 381-8550, Japan
[10] Tokyo Metropolitan College of Industrial Technology, Tokyo 116-8523, Japan
[11] School of Chemical and Physical Sciences, Victoria University, Wellington, New Zealand
[12] Mt. John University Observatory, University of Canterbury, P.O. Box 56, Lake Tekapo 8770, New Zealand
[13] Universidad de Concepción, Departamento de Astronomia, Casilla 160-C, Concepción, Chile
[14] Institute of Astronomy, University of Cambridge, Madingley Road, Cambridge CB3 0HA, UK
[15] Department of Astronomy, The Ohio State University, 140 West 18th Avenue, Columbus, OH 43210, USA

ABSTRACT

We report on the analysis of the high microlensing event MOA-2008-BLG-379, which has a strong microlensing anomaly at its peak due to a massive planet with a mass ratio of $q = 6.9 \times 10^{-3}$. Because the faint source star crosses the large resonant caustic, the planetary signal dominates the light curve. This is unusual for planetary microlensing events, and as a result, the planetary nature of this light curve was not immediately noticed. The planetary nature of the event was found when the Microlensing Observations in Astrophysics (MOA) Collaboration conducted a systematic study of binary microlensing events previously identified by the MOA alert system. We have conducted a Bayesian analysis based on a standard Galactic model to estimate the physical parameters of the lens system. This yields a host star mass of $M_L = 3.3^{+1.7}_{-1.2} \, M_\odot$ orbited by a planet of mass $m_P = 0.56^{+0.24}_{-0.27} \, M_{\rm Jup}$ at an orbital separation of $a = 3.3^{+1.3}_{-1.2}$ AU at a distance of $D_L = 4.1^{+1.7}_{-1.9}$ kpc. The faint source magnitude of $I_S = 21.30$ and relatively high lens-source relative proper motion of $\mu_{\rm rel} = 7.6 \pm 1.6$ mas yr^{-1} imply that high angular resolution adaptive optics or *Hubble Space Telescope* observations are likely to be able to detect the source star, which would determine the masses and distance of the planet and its host star.

Key word: gravitational lensing: micro

Online-only material: color figures

1. INTRODUCTION

Since the first discovery of an extrasolar planet orbiting an ordinary star in 1995 (Mayor & Queloz 1995), more than 1000 planets have been found to date. Most of the planets discovered were through the radial velocity (Butler et al. 2006; Bonfils et al. 2013) and transit (Borucki et al. 2011) methods, which are the most sensitive to planets orbiting close to their host stars. In contrast, direct imaging is the most sensitive to young planets in orbits wider than that of Saturn (Marois et al. 2008). The gravitational microlensing method has unique sensitivity to the planets orbiting just outside of the snow line with masses down to Earth mass (Bennett & Rhie 1996). The snow line (Ida & Lin 2005; Lecar et al. 2006; Kennedy et al. 2006; Kennedy &

Kenyon 2008; Thommes et al. 2008) plays a critical role in the core accretion theory of planet formation. Ices, including water ice, can condense beyond the snow line, which increases the density of solid material in the proto-planetary disk by a factor of a few, compared to the disk just inside the snow line. The higher density of solids means that the solid planetary cores can form more quickly beyond the snow line, so microlensing is unique in its ability to probe the planetary mass function at the separation where planet formation is thought to be the most efficient.

To date, the primary contribution of the microlensing method to the study of exoplanets is the statistical results indicating that cold planets in wide orbits are quite common (Sumi et al. 2010; Gould et al. 2010b; Cassan et al. 2012). Relatively low-mass cold Neptunes or super-Earths are found to be more common than gas giants, which is in rough agreement with the core accretion theory expectation. Microlensing is also unique in its sensitivity to planets orbiting stars that are too faint to detect

---

[16] Microlensing Observations in Astrophysics (MOA) Collaboration.
[17] Optical Gravitational Lensing Experiment (OGLE) Collaboration.

(Bennett 2008; Gaudi 2012). In fact, planetary mass objects can be detected even in cases when there is no indication of a host star (Sumi et al. 2011).

The microlensing events that are monitored for the signals of extrasolar planets are mainly identified by the two main microlensing survey groups, the Microlensing Observations in Astrophysics (MOA; Bond et al. 2001; Sumi et al. 2003) and the Optical Gravitational Lensing Experiment (OGLE; Udalski 2003). The MOA survey uses the MOA-II 1.8 m telescope with a 2.2 deg^2 field-of-view (FOV) CCD camera MOA-cam3 (Sako et al. 2008) at Mt. John University Observatory in New Zealand. With this large FOV camera, MOA is able to observe >40 deg^2 of the central Galactic bulge fields every hour, with a higher cadence for the fields with the largest microlensing rate. MOA identifies about 600 microlensing events in progress each year and issues public alert messages as each new event is identified. The OGLE survey has been conducted with the 1.3 m Warsaw Telescope at the Las Campanas Observatory in Chile, which is currently equipped with a 1.4 deg^2 CCD mosaic camera. However, in 2008, when the microlensing event MOA-2008-BLG-379 took place, OGLE was operating the OGLE-III survey using a camera with a 0.35 deg^2 FOV. OGLE-III typically identified ∼100 more events than MOA-II, but observed at a lower cadence with most fields only being observed once per night. Currently, the OGLE-IV survey operates at a relatively high cadence in the central Galactic bulge, but covers a much wider area of sky at a lower cadence, which yields nearly 2000 microlensing event discoveries per year. Most recently, the Wise microlensing survey (Shvartzvald & Maoz 2012) has conducted high cadence observations using a 1.0 deg^2 CCD mosaic camera on the 1.0 m Wise Telescope in Israel. They fill the gap in longitude between MOA and OGLE, but due to their Northerly location, they can only observe the Galactic bulge for a limited amount of time each night.

Microlensing follow-up groups, such as μFUN, PLANET, RoboNet, and MINDSTEp, observe microlensing events that have been previously identified by one or more of the survey groups. They aim to ensure dense, 24 hr light curve coverage on the highest priority microlensing events, and they contribute to planet discoveries in a number of ways. They can identify planetary signals in some of the microlensing events with relatively bright source stars (Beaulieu et al. 2006; Batista et al. 2011), densely monitor high magnification microlensing events (Udalski et al. 2005; Gould et al. 2010b; Miyake et al. 2011; Bachelet et al. 2012; Yee et al. 2012; Han et al. 2013) that are known to have high sensitivity to planets (Griest & Safizadeh 1998; Rhie et al. 2000), or follow-up on events once potential planetary anomalies have been found by the survey teams (Sumi et al. 2010; Muraki et al. 2011; Kains et al. 2013). In addition, some events have been identified based on higher cadence observations by the survey groups prompted by the real-time identification of potential planetary anomalies (Bond et al. 2004). However, if the survey cadence is high enough, it is possible to identify planets from survey observations alone without the benefit of follow-up observations from either the survey or follow-up teams. The event we present here, MOA-2008-BLG-379, is the planetary microlensing event that was found based on survey observations alone, similar to MOA-2007-BLG-192 (Bennett et al. 2008), MOA-bin-1 (Bennett et al. 2012) and MOA-2011-BLG-322 (Shvartzvald et al. 2013). We should note that there are many more planetary events, such as MOA-2011-BLG-293 (Yee et al. 2012) and OGLE-2012-BLG-0406 (Poleski et al. 2013), that could have

been discovered based upon survey observations alone. And in fact, the primary reason for the lack of follow-up observations for MOA-2007-BLG-192 and MOA-2008-BLG-379 is the lack of experience in the microlensing community with the full range of possible planetary signals.

In this paper, we report on the analysis of a planetary microlensing event MOA-2008-BLG-379. Section 2 describes the observations of this event, and Section 3 describes the reduction of the data and the light curve modeling. In Section 4, source magnitude and color measurement using color–magnitude diagram (CMD) is discussed, and the derived angular Einstein radius is discussed in Section 5. In Section 6, we use a Bayesian analysis based on a standard Galactic model to estimate the masses and distances of the lens system based on the angular Einstein radius. Discussion and our conclusions are presented in Section 7.

2. OBSERVATIONS

Prior to 2009, the MOA-II observing strategy called for the observations of the two fields with the highest lensing rate every 10 minutes and observations of the remaining 20 fields every hour using the custom wide-band MOA-Red filter, which is roughly the sum of the Cousins R- and I-bands. MOA-2008-BLG-379 was discovered in field gb8, which was observed with an hourly cadence in 2006–2008.

The microlensing event MOA-2008-BLG-379 was identified by the MOA alert system (Bond et al. 2001) at (R.A., decl.) (J2000) = ($17^h58^m49^s.44$, $−30°11'48''.95$), and was announced by the MOA collaboration at UT 22:00, 2008 August 9, (or HJD$'$ = 4688.42). As can be seen from the light curve in Figure 1, this was after the first caustic entrance and exit and the central cusp approach feature. Given the sparse coverage and lack of OGLE data at this time, it was not immediately obvious that this event was anomalous. Two weeks later, at UT 20:00 2008 August 23, the event was also identified and announced by the OGLE Early Warning System (EWS; Udalski et al. 1994) as OGLE-2008-BLG-570. The delay in the identification of this event by OGLE was due to the fact that the source was faint and was not located close to the location of a "star" that was identified in the OGLE reference image. This is fairly common, as most bulge main sequence stars are not individually resolved at ∼1″ resolution. The source star, MOA-2008-BLG-379S, happens to be located at an unusually large distance from the nearest star in the OGLE catalog, and as a result, it could only be found via the "new object" channel of the OGLE EWS. In 2008 this channel was not run as often as the regular "resolved star" channel of the OGLE EWS. As a result, both the MOA and OGLE collaboration groups observed this event with normal cadence.

3. DATA REDUCTION AND MODELING

The MOA and OGLE data for MOA-2008-BLG-379 were reduced using the respective MOA (Bond et al. 2001) and OGLE (Udalski 2003) photometry pipelines. The initial reductions used the normal photometry available on the respective MOA and OGLE alert web sites, and these data were used to show that the correct model involved a planet. However, it was possible to obtain improved photometry for both the MOA and OGLE data sets. The improved MOA photometry used "cameo" sub-images centered on the target, and the improved OGLE photometry was redone with source position determined from difference images and a careful selection of reference images.
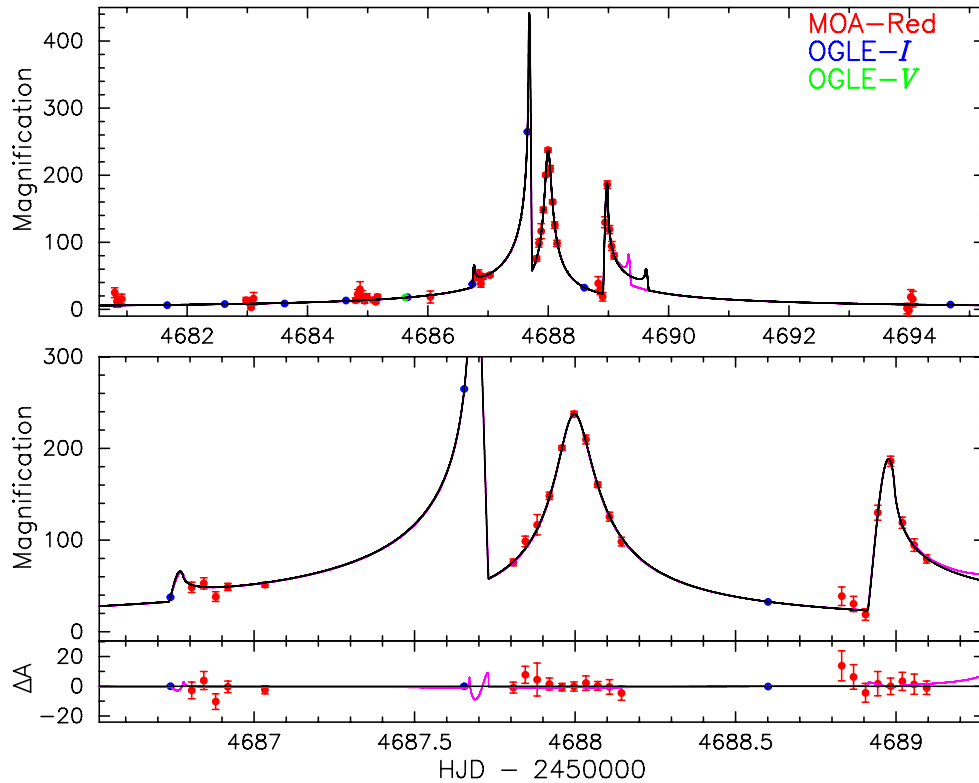
Figure 1. Light curve of MOA-2008-BLG-379. The top panel shows the magnified part of the light curve and the middle panel shows a close up of the anomaly. The red, blue, and green points are for MOA-Red, OGLE-*I*, and OGLE-*V*, respectively. The black and magenta lines indicate the best close and wide model. The bottom panel shows the residual from the best close model.

Table 1
The Error Bar Corrections Parameters and Linear Limb Darkening Parameters for the Data Sets Used to Model the MOA-2008-BLG-379 Light Curve

Dataset	k	$e_{\min}$	Limb-darkening Coefficients	Number of Data
MOA-Red	1.266	0	0.5919	951
OGLE *I*-band	0.995	0	0.5493	294
OGLE *V*-band	1.180	0	0.7107	7

Notes. The formula used to modify the error bars is $\sigma_i' = k\sqrt{\sigma_i^2 + e_{\min}^2}$ where σ_i is the input error bar for the ith data point from the photometry code in magnitudes, and σ_i' is the final error bar used for the determination of parameter uncertainties.

Both the OGLE and MOA photometry were found to have systematic errors at the beginning and/or end of each observing season when observations are only possible at high airmass. This may be due to low-level variability for a very bright star about 3 arcseconds from the source, MOA-2008-BLG-379S. So we removed the MOA data prior to HJD′ = HJD − 2450000 = 4543, leaving 951 MOA data points in the range $4543 < \text{HJD}' < 4762$. The OGLE data consist of 294 *I*-band observations and 7 *V*-band observations, as shown in Table 1.

The error bar estimates from the photometry codes are normally accurate to a factor of two or better, and they provide a good estimate of the relative photometry errors for each data set. These are sufficient to find the best light curve model, but in order to estimate the fit parameter uncertainties, we need more accurate error bars, which have $\chi^2/\text{dof} \simeq 1$ for each data set. Therefore, once we have found the best fit model with the unmodified error bars, we modify the error bars with the formula

$$\sigma_i' = k\sqrt{\sigma_i^2 + e_{\min}^2} \qquad (1)$$

where σ_i is the input error bar estimate (in magnitudes) for the ith data point, k is the normalization factor, and $e_{\min}$ is the minimum error. The modified error bars, σ_i', are used for all subsequent modeling and parameter uncertainty determination.

The factors k and $e_{\min}$ are estimated for each data set with the following procedure. First, we plot the cumulative distribution of χ^2 as a function of the size of the input error bars, σ_i. Then, we chose the value of $e_{\min} \geqslant 0$ such that the cumulative distribution is a straight line with slope of unity. Then, the parameter k is chosen to give $\chi^2/\text{dof} \simeq 1$ for each data set. For this event, we find that $e_{\min} = 0$ for all data sets. The values of k and $e_{\min}$ for all three data sets are listed in Table 1.

This event was identified in a systematic modeling of all anomalous events (i.e., those not well fit by a point source, single lens model without microlensing parallax) from the MOA alert pages (https://it019909.massey.ac.nz/moa/) from the 2007–2010 seasons. A similar analysis of OGLE-III binary events was conducted by Jaroszyński et al. (2010). The light curve calculations for this systematic analysis were done using the image centered ray-shooting method (Bennett & Rhie 1996; Bennett 2010). All the events that have anomalous deviation from a point source, single lens model were fitted with the binary lens model according to the following procedure. Binary lens models have three parameters that are in common with single lens models. These parameters are the time of the closest approach to the lens system center of mass t_0, the Einstein radius crossing time, t_E, and the impact parameter u_0, in units of the angular Einstein radius θ_E. Binary lens models also require three additional parameters. These are the lens system planet-star mass ratio, q, the planet-star separation, s, projected into the plane perpendicular to the line-of-sight, and the angle of the source trajectory relative to the binary lens axis α. Another parameter, the source radius crossing time, t_* is also included
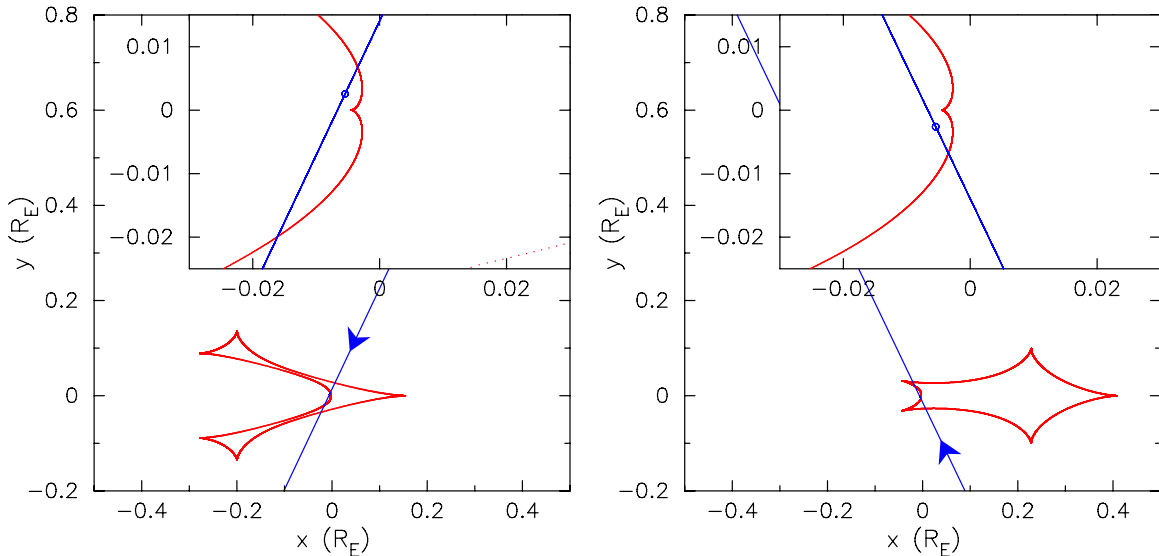
Figure 2. Caustic geometries for both close (left) and wide (right) models are indicated by the red curves. The insets in each panel are close up around the center of the coordinate. The blue lines show the source star trajectory with respect to the lens system, with arrows indicating the direction of motion. The small blue circles in the insets indicate the source star size.

(A color version of this figure is available in the online journal.)

in the binary lens model because this parameter is important for most of planetary microlensing light curves. We carefully searched to find the best fit binary lens model over a wide range of values of microlensing parameters using a variation of the Markov Chain Monte Carlo (MCMC) algorithm (Verde et al. 2003). Because the shape of anomaly features in the light curve well depends on q, s and α, these three parameters are fixed in the first search. Next, we searched χ^2 minima of the 100 models in order of χ^2 in the first search with each parameter free and found the best fit model.

This analysis indicated a planetary mass ratio for the MOA-2008-BLG-379L lens system. Figure 1 shows the light curve of this event and the best fit models. There are five distinct caustic crossing and cusp approach features in the light curve. The first caustic crossing is sandwiched between a single observation by OGLE and five MOA observations beginning 96 minutes later at HJD$'$ = 4686.8, The subsequent, very bright, caustic exit was observed with a single OGLE observation on the subsequent night, but the central cusp approach feature and the next caustic entrance feature were reasonably well sampled by 9 and 7 MOA observations, respectively, on the next two nights. It is the sampling of these two features that allow the parameters of the planetary lens model for this event to be determined.

For many binary events and most planetary events, the light curve has very sharp features due to caustic crossings or cusp approaches that resolve the finite size of the source star. Such features require an additional parameter, the source radius crossing time, t_*. Since the MOA-2008-BLG-379 includes caustic crossings and a close cusp approach, it is necessary to include finite source effects in its light curve model, and a proper accounting of finite source effects requires that limb darkening be included.

For the limb darkening coefficients, we adopted a linear limb-darkening model for the source star based on the source color estimate of $(V - I)_{S,0} = 0.81 \pm 0.13$, which is discussed below in Section 4. This color implies that the source is a late G-star with an effective temperature of $T_{\rm eff} \simeq 5386$ K (Bessell & Brett 1988). We use limb-darkening parameters from Claret (2000) for a source star with an effective temperature

$T_{\rm eff} = 5500$ K, surface gravity $\log g = 4.5$ cm s^{-2}, and metallicity $\log[{\rm M/H}] = 0.0$. Girardi's isochrones (Girardi et al. 2002) suggest that the source may be a metal poor star if it is located at the distance of the Galactic center, but $\log[{\rm M/H}] = 0.0$ is consistent within the 1σ error bar. The list of the coefficients used for the linear limb-darkening model are as follows, 0.7107 for V, 0.5493 for I, and 0.5919 for MOA-Red, which is the mean of the coefficients for the Cousins R and I-bands. These are listed in Table 1.

As is commonly the case for high magnification events, there are two degenerate light curve solutions that can explain the observed light curve. This is the well-known "close-wide" degeneracy, where the solutions have nearly identical parameters except that the separation is modified by the $s \leftrightarrow 1/s$ transformation. Figure 2 shows the two caustic configurations from the close and wide models for this event. Sometimes, when the planetary caustics have merged with the central caustic to form a so-called resonant caustic curve, as in this case, the light curve data can resolve this close-wide degeneracy. We can see in Figure 1 that the close and wide light curves do have substantial differences, such as the time of the final caustic exit. However, the observations for this event are too sparse to sample these light curve features, and the degeneracy remains. Fortunately, the parameters for these two solutions differ by only $\sim 20\%$, so this degeneracy has little effect on the inferred physical parameters of the lens system. We find $s = 0.903 \pm 0.001$, $q = (6.85 \pm 0.05) \times 10^{-3}$ and $u_0 = (6.02 \pm 0.06) \times 10^{-3}$ for the close model, which is preferred by $\Delta\chi^2 = 0.7$, and $s = 1.119 \pm 0.001$, $q = (6.99 \pm 0.01) \times 10^{-3}$, and $u_0 = (-6.03 \pm 0.03) \times 10^{-3}$ for the wide model. The full set of fit parameters are listed in Table 2.

Higher order effects such as microlens parallax, xallarap (source star orbital motion) and orbital motion in the lens system have been detected in some previous events(Alcock et al. 1995; Gaudi et al. 2008; Bennett et al. 2010; Sumi et al. 2010; Muraki et al. 2011; Kains et al. 2013). The measurement of finite source effects or microlensing parallax effects can partially break the degeneracies of the physical parameters that can be inferred from the microlensing light curve, and the measurement of both

Table 2
The Best Fit Model Parameters for Both the Wide and Close Models

Model	t_0 HJD′	t_E (days)	u_0 10^{-3}	q 10^{-3}	s	θ (rad)	t_* (days)	χ^2
Wide	4687.896	42.14	6.03	6.99	1.119	1.124	0.0219	1246.7
	0.001	0.23	0.03	0.01	0.001	0.003	0.0020	
Close	4687.897	42.46	6.02	6.85	0.903	5.154	0.0212	1246.0
	0.001	0.45	0.06	0.05	0.001	0.002	0.0017	

Notes. The second and fourth rows in each column are the 1σ error bars for each parameter. HJD′ ≡ HJD − 2450000.

microlensing parallax and finite source effects yields a direct measurement of the lens system mass (Bennett 2008; Gaudi 2012). For this event, however, the source is too faint for a reliable microlensing parallax measurement for an event of its duration, and the relatively sparse data sampling leaves some uncertainty in the measurement of the source radius crossing time. Therefore, we use the light curve constraints on the source radius crossing time to constrain the physical parameters of the lens system using a Bayesian analysis based on a standard Galactic model, as discussed in Section 6. If the lens star can be detected in high angular resolution follow-up observations, it will then be possible to directly determine the physical parameters of the lens system (Bennett et al. 2006, 2007; Dong et al. 2009).

4. SOURCE COLOR AND MAGNITUDE

The source star magnitude and color estimated from the light curve modeling are affected by extinction and reddening due to interstellar dust. These effects must be removed in order to infer the intrinsic brightness and color of the source star. In order to estimate extinction and reddening, we use the centroid of the red clump giant (RCG) distribution, which is an approximate standard candle. The CMD, shown in Figure 3 was made from stars from the OGLE-III catalog (Szymański et al. 2011) within 2′ from the source star. From this CMD, we have found the RCG centroid to be at

$$(V - I, I)_{\rm RCG} = (2.55, 16.24) \pm (0.02, 0.04) . \qquad (2)$$

We adopt the intrinsic RCG centroid $V - I$ color and magnitude from Bensby et al. (2011) and Nataf et al. (2013), respectively, which gives

$$(V - I, I)_{\rm RCG,0} = (1.06, 14.42) \pm (0.06, 0.04) . \qquad (3)$$

Comparing our measured RCG centroid from Equation (2) with the intrinsic dereddened magnitude and extinction from Equation (3), we find that the reddening and extinction are

$$(E(V - I), A_I)_{\rm RCG} = (1.49, 1.82) \pm (0.06, 0.06), \qquad (4)$$

where $E(V - I)$ is the average reddening and A_I is the average extinction.

The models presented in Table 2 give the source magnitude and color of $I_S = 21.30 \pm 0.03$ and $(V - I)_S = 2.07 \pm 0.09$ from the OGLE observations, calibrated to the OGLE-III photometry map (Szymański et al. 2011). This color is bluer than most of the bulge main sequence stars at this magnitude, but with the error bars, it is marginally consistent with a bulge main sequence star, as shown in Figure 3. This could be due to the fact that there is only a single bright OGLE V-band image that might be affected by a nearby bright variable star.
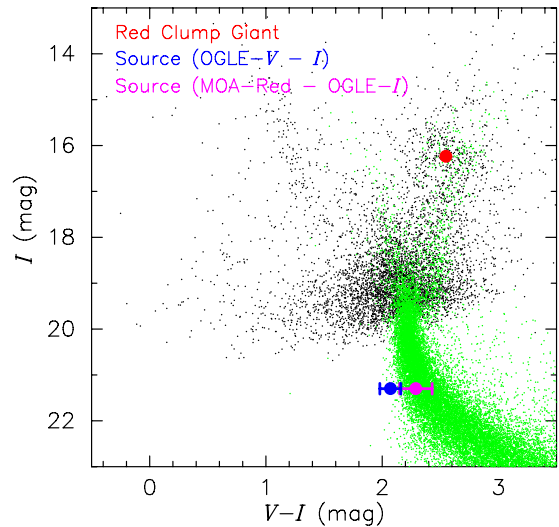

Figure 3. Color–magnitude diagram (CMD) of the stars within 2′ of MOA-2008-BLG-379 from the OGLE-III catalog is shown as black dots. The green dots show the *HST* CMD of Holtzman et al. (1998) whose extinction is adjusted to match the MOA-2008-BLG-379 using the Holtzman field red clump giant (RCG) centroid of $(V - I, I)_{\rm RCG,Holtz} = (15.15, 1.62)$ (Bennett et al. 2008). The red dot indicates the RCG centroid for the MOA-2008-BLG-379 field. The source star color and magnitude derived from OGLE $V I$ is indicated with a blue dot, while the source star color and magnitude derived from the MOA-Red and OGLE-I passbands is shown as a magenta dot. Although the error bars on the MOA-Red + OGLE-I color estimate are similar to the error bar from the OGLE $V I$ estimate, we use the MOA-Red + OGLE-I estimate for the source color because it is subject to smaller systematic uncertainties.
(A color version of this figure is available in the online journal.)

Because the MOA-Red passband is centered at a slightly shorter wavelength than the OGLE I-band, we can use the MOA-Red and OGLE I passbands to derive the source color (Gould et al. 2010a). Although the color difference between these two passbands is relatively small, we have a large number of data points at significant magnification in both of these passbands. So, this method should yield a color that is less sensitive to systematic photometry errors than the determination based on the single magnified OGLE V-band measurement. In order to calibrate the MOA-Red measurements to the OGLE-III (V, I) system, we use the OGLE-III photometry map (Szymański et al. 2011) and a DoPHOT (Schechter et al. 1993) reduction of the MOA reference frame. Because the seeing in the MOA reference frame is significantly worse than the seeing images used for the OGLE-III catalog, we choose isolated OGLE stars for the comparison with MOA to avoid problems due to blending in the MOA images. In order to select the stars with small uncertainty in magnitude and color, we remove faint stars with $I > 19$ and stars with a $V - I$ error bar > 0.1. In order to obtain an accurate linear relation, we only fit stars in the color range $2 < V - I < 4$. We recursively reject 2.5σ outliers and find

$$R_{M,\rm DoPHOT} - I_{\rm OGLE-III} = (0.18931 \pm 0.00533)(V - I)_{\rm OGLE-III}, \qquad (5)$$

where $I_{\rm OGLE-III}$ and $V_{\rm OGLE-III}$ are the OGLE-III catalog magnitudes, and $R_{M,\rm DoPHOT}$ is the calibrated MOA-Red band magnitude. (The MOA-Red calibration has a zero-point uncertainty of 0.0144 mag.) The MOA light curve photometry (Bond et al. 2001) is done with the difference imaging analysis (DIA; Tomaney & Crotts 1996; Alard & Lupton 1998), which is usually significantly more precise than DoPHOT, but DIA only

measures changes in brightness, which is why DoPHOT photometry is used to derive the relation in Equation (5) between the $R_M - I_{OGLE}$ and standard $V - I$ colors. Thus, it is important that the MOA-Red band photometry from the DIA and DoPHOT codes have identical magnitude scales. This is accomplished by using the DoPHOT point-spread function for the DIA photometry. Using the source magnitudes from the light curve modeling, this procedure yields $(V - I, I)_S = (2.29, 21.30) \pm (0.14, 0.03)$ for the best fit model. As shown in Figure 3, this source magnitude and color are more reasonable for a bulge source than the less precise color derived from OGLE V-band measurements, and it is the one that we use in our analysis.

Combining the extinction from Equation (4) with the source magnitudes and colors from the best fit wide and close models, we have

$$(V - I, I)_{S,0} = (0.79, 19.48)$$
$$\pm (0.13, 0.06) \text{ for the wide model} \quad (6)$$

$$(V - I, I)_{S,0} = (0.80, 19.49)$$
$$\pm (0.12, 0.06) \text{ for the close model.} \quad (7)$$

Also, from the light curve models, we have determined the magnitude of the unlensed flux at the location of the source. This is the flux of the stars with images blended with the source. The flux from the blend stars is often used as an upper limit for the magnitude of the lens star. In this event, however, we found that the blending flux in the light curve is dominated by the flux from a bright star $0\rlap.''5$ away from the event by careful inspection of the OGLE reference image. We found that no star is resolved at the position of the event and thus the real upper limit of the lens magnitude is fainter. If we assume that the extinction to these blend stars is the same as the source (which is a reasonable approximation if the stars are at a distance of $\gtrsim 4$ kpc), then we have the extinction-free 3σ limit of blend magnitude

$$I_{b,0} > 17.87 \text{ mag} \quad (8)$$

which will be used as an upper limit for the magnitude of the planetary host star in Section 6.

5. ANGULAR EINSTEIN RADIUS θ_E

With the use of $(V - I, I)_{S,0}$, we can determine the source angular radius with the color surface–brightness relation of Kervella & Fouqué (2008),

$$\log_{10}(2\theta_*) = 0.4992 + 0.6895(V - I) - 0.0657(V - I)^2 - 0.2V . \quad (9)$$

This yields an angular source radius of $\theta_* = 0.45 \pm 0.07 \ \mu as$. θ_* is also able to be derived from the method of Kervella et al. (2004) with $(V - K)_{S,0}$ estimated from the dwarf star color–color relations from Bessell & Brett (1988), but the result is consistent with the above value. We can combine this value of θ_* with the fit source radius crossing time, t_*, values from the light curve models to determine the lens-source relative proper motion,

$$\mu_{rel} = \frac{\theta_*}{t_*} = \frac{\theta_E}{t_E}$$
$$= 7.46 \pm 1.65 \text{ mas yr}^{-1} \text{ for the wide model} \quad (10)$$
$$= 7.75 \pm 1.56 \text{ mas yr}^{-1} \text{ for the close model.} \quad (11)$$

Note that this is the relative proper motion in the instantaneously geocentric inertial reference frame that moved with the Earth when the event reached peak magnification. The measurement of t_* also yields the angular Einstein radius

$$\theta_E = \frac{\theta_* t_E}{t_*} = 0.86 \pm 0.19 \text{ mas for the wide model} \quad (12)$$
$$= 0.90 \pm 0.18 \text{ mas for the close model,} \quad (13)$$

which can be used to help constrain the lens mass.

As we discuss in Section 7, follow-up observations might be able to detect the lens separating the source and measure the lens-source relative proper motion. However, this would be in the heliocentric reference frame rather than the instantaneously geocentric inertial frame used for Equations (10) and (11). Fortunately, the follow-up observations and light curve model provide enough information to convert between these two reference frames.

For this paper, however, we have not been able to distinguish the wide and close models, so to obtain our final predictions, we combine the values from the wide and close models with weights given by $e^{-\Delta\chi^2/2}$. This gives an angular Einstein radius and lens-source relative proper motion of

$$\theta_E = 0.88 \pm 0.19 \text{ mas} \quad (14)$$
$$\mu_{rel} = 7.63 \pm 1.61 \text{ mas yr}^{-1}, \quad (15)$$

with the lens-source relative proper motion in the same instantaneous geocentric inertial reference frame used for Equations (10) and (11).

6. BAYESIAN ANALYSIS

A microlensing light curve for a single lens event normally has the lens distance, mass, and angular velocity with respect to the source constrained by only a single measured parameter, the Einstein radius crossing time, t_E. But, like most planetary microlensing events, MOA-2008-BLG-379 has finite source effects that allow t_*, and therefore θ_E, to be measured. If we could have also measured the microlensing parallax effect, we could determine the total lens system mass (Bennett 2008; Gaudi 2012).

Without a microlensing parallax measurement, we are left with the relation

$$\theta_E^2 = \kappa M \left(\frac{1}{D_L} - \frac{1}{D_S} \right) \quad (16)$$

where $\kappa = 8.14 \text{ mas}/M_\odot$, M is the mass of the lens system, and D_S is the distance to the source star. This can be interpreted as a lens mass–distance relation, since D_S is approximately known.

We can now use this mass–distance relation, Equation (16), in a Bayesian analysis to estimate the physical properties of the lens system (Beaulieu et al. 2006). Our Bayesian analysis used the Galactic model of Han & Gould (2003) with an assumed Galactic center distance of 8 kpc with model parameters selected from the MCMC used to find the best fit model. The lens magnitude is constrained to be less than the blend magnitudes presented in Equation (8). Since the best fit wide model is slightly disfavored by $\Delta\chi^2 = 0.7$, we weight the wide model Markov chains by $e^{-\Delta\chi^2/2}$ with respect to the close model Markov chains. The probability distributions resulting from this Bayesian analysis are shown in Figures 4 and 5.

An important caveat to this Bayesian analysis is that we have assumed that stars of all masses, as well as brown dwarfs,
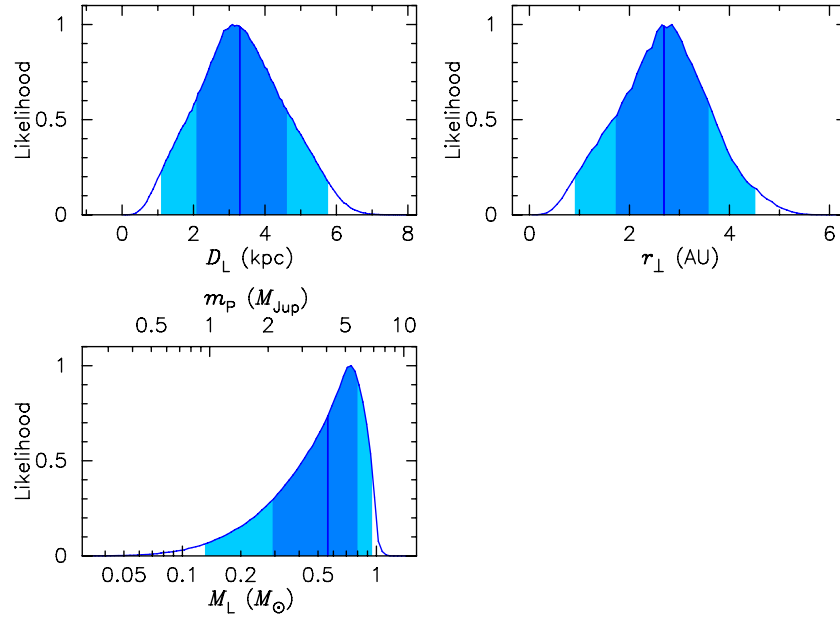
Figure 4. Probability distribution of lens parameters from the Bayesian analysis. The top-left panel shows the probability of the distance to the lens system. The bottom-left panel shows the mass of the primary and secondary lenses (the star and planet) in units of Solar and Jupiter masses, respectively. The top-right panel shows the projected separation $r_\perp$. The dark and light blue regions indicate the 68% and 95% confidence intervals, and the vertical lines indicate the median value.

(A color version of this figure is available in the online journal.)
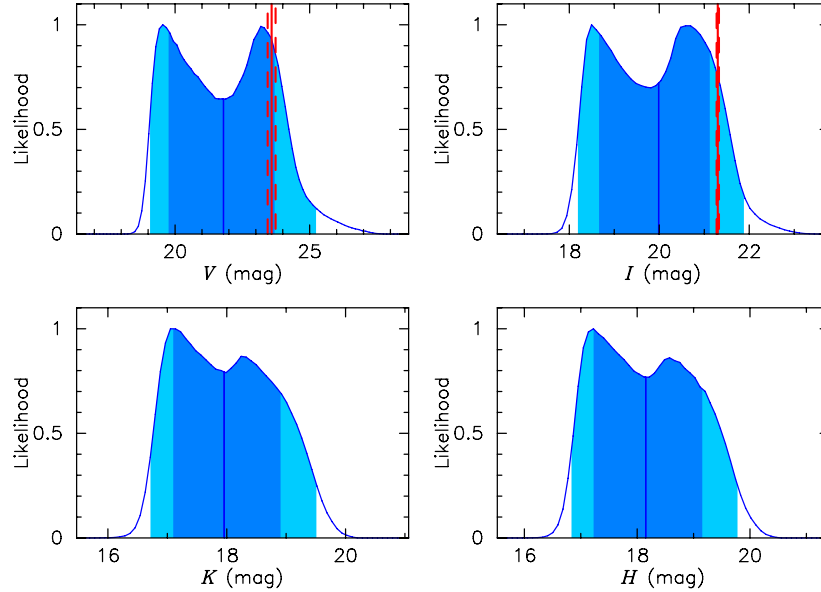
Figure 5. Probability distribution of V-, I-, K- and H-band magnitudes for the extinction-free lens star from the Bayesian analysis. The dark and light blue regions indicate the 68% and 95% confidence intervals. The red solid lines show the source star magnitudes with the extinction estimated in Equation (4), and the red dashed lines are their 1 sigma errors.

(A color version of this figure is available in the online journal.)

Table 3
Physical Parameters of the Lens System Obtained from the Bayesian Analysis

Primary Mass M_L ($M_\odot$)	Secondary Mass m_P (M_{Jup})	Distance D_L (kpc)	Projected Separation $r_\perp$ (AU)	Separation a (AU)
$0.56^{+0.24}_{-0.27}$	$4.1^{+1.7}_{-1.9}$	$3.3^{+1.3}_{-1.2}$	$2.7^{+0.9}_{-1.0}$	$3.3^{+1.7}_{-1.2}$

are equally likely to host a planet with the measured mass ratio and separation. Because of this assumption, the results of this Bayesian analysis cannot (directly) be used to determine the probability that stars will host planets as a function of their mass. With this caveat, the star and planet masses re-

sulting from the Bayesian analysis are $M_L = 0.56^{+0.24}_{-0.27}\ M_\odot$ and $m_P = 4.1^{+1.7}_{-1.9}\ M_{Jup}$, respectively. Their projected separation was determined to be $r_\perp = 2.7^{+0.9}_{-1.0}$ AU, and the lens system is at a distance of $D_L = 3.3^{+1.3}_{-1.2}$ kpc. The three-dimensional star-planet separation is estimated to be $a = 3.3^{+1.7}_{-1.2}$ AU, assuming a random inclination and phase. These values are listed in Table 3. Therefore, the most likely physical parameters from the Bayesian analysis, indicate that the planet has a mass of nearly 4 Jupiter masses and orbits a late K-dwarf host star at just over twice the distance of the snow line.

7. DISCUSSION AND CONCLUSION

We reported on the discovery and analysis of a planetary microlensing event MOA-2008-BLG-379. As is often the case with high magnification microlensing events, there are two degenerate models: a close model with a planet-host separation of $s = 0.903$ and a wide model with $s = 1.119$. Both have a mass ratio of $q \simeq 7 \times 10^{-3}$. Our Bayesian analysis indicates that the lens system consists of a G, K, or M-dwarf orbited by a super-Jupiter mass planet. The most likely physical properties for the lens system, according to the Bayesian analysis, are that the host is a late K-dwarf, and the planet has a mass of about 4 Jupiter masses with a projected separation of about 3 AU. However, these values are dependent on our prior assumption that stars of different masses have equal probabilities to host a planet of the observed mass ratio and separation.

Fortunately, the parameters of this event are quite favorable for a direct determination of the lens system mass and distance by the detection of the lens separating from the source star in high angular resolution follow-up observations (Bennett et al. 2006, 2007). The source star is quite faint at $I_S = 21.30 \pm 0.03$, so it is unlikely that the lens will be very much fainter than the source. The brightness of the source is compared to the Bayesian analysis predictions for the lens (host) star in the V-, I-, H-, and K-bands in Figure 5. This indicates that the lens star is likely to have a similar brightness to the source in all of these passbands. Also, it is unlikely that the lens and source magnitudes will differ by more than 2 mag in any of these passbands, so both the source and lens should be detectable.

The measured source radius crossing time indicates a relatively large lens-source relative proper motion of $\mu_{\rm rel} = 7.6 \pm 1.6$ mas yr^{-1} (measured in the inertial geocentric reference frame moving at the velocity of the Earth at the peak of the event). This implies a separation of $\sim 37.8 \pm 8.3$ mas in the later half of 2013 when high resolution follow-up observations were obtained from Keck and the *Hubble Space Telescope* (*HST*). (Because the relative proper motion, $\mu_{\rm rel}$, is measured in an instantaneously geocentric reference frame, it cannot be directly converted into a precise separation prediction, but the conversion to the heliocentric reference frame, which is more relevant to the follow-up observation, usually results in a small change.) The results of these follow-up observations will be reported in a future publication, but it seems quite likely that the planetary host star will be detected, resulting in a complete solution of the lens system. That is, the lens masses, distance and separation will all be determined in physical units.

One unfortunate feature of this discovery is that MOA-2008-BLG-379 was not recognized as a planetary microlensing event when it was observed. This was partly due to the faintness of the source star, which rendered the relatively long planetary perturbation as the dominant portion of the magnified light curve. However, the lack of familiarity with the complete variety of binary lens and planetary microlensing light curves also played a role in this lack of recognition. The planetary nature of the event was discovered as a result of a systematic effort to model all of the binary microlensing events that were found by the MOA alert system. Fortunately, the joint analysis of OGLE data and the high cadence MOA-II survey observations allowed the planetary nature of the event to be establish and the basic planetary lens parameters to be measured.

The MOA-II high cadence survey was enabled by the wide, 2.2 deg^2 field MOA-cam3 that enabled hourly survey observations. In 2010 March, the OGLE group started the OGLE-IV survey with their new 1.4 deg^2 CCD camera, and they now also conduct a high cadence survey of the central Galactic bulge. This new camera and the good seeing available at the OGLE site (Las Campanas) has substantially increased the rate in which planetary deviations are discovered in survey observations. The combination of the MOA-II and OGLE-IV high cadence surveys greatly improves the light curve sampling of these survey microlensing planet discoveries due to the large separation in longitude between the MOA and OGLE telescopes. The capabilities of microlensing follow-up teams are also rapidly improving, most notably with the recent expansion (Brown et al. 2013) of the Las Cumbres Observatory Global Telescope Network, which should result in much higher light curve sampling rates of planetary signals discovered in progress.

REFERENCES

Alard, C., & Lupton, R. H. 1998, ApJ, 503, 325
Alcock, C., Allsman, R. A., Alves, D., et al. 1995, ApJL, 454, L125
Bachelet, E., Fouqué, P., Han, C., et al. 2012, A&A, 547, A55
Batista, V., Gould, A., Dieters, S., et al. 2011, A&A, 529, A102
Beaulieu, J.-P., Bennett, D. P., Fouqué, P., et al. 2006, Natur, 439, 437
Bennett, D. P 2008, in Exoplanets, ed. J. Mason (Berlin: Springer), 47
Bennett, D. P. 2010, ApJ, 716, 1408
Bennett, D. P., Anderson, J., Bond, I. A., Udalski, A., & Gould, A. 2006, ApJL, 647, L171
Bennett, D. P., Anderson, J., & Gaudi, B. S. 2007, ApJ, 660, 781
Bennett, D. P., Bond, I. A., Udalski, A., et al. 2008, ApJ, 684, 663
Bennett, D. P., & Rhie, S. H. 1996, ApJ, 472, 660
Bennett, D. P., Rhie, S. H., Nikolaev, S., et al. 2010, ApJ, 713, 837
Bennett, D. P., Sumi, T., Bond, I. A., et al. 2012, ApJ, 757, 119
Bensby, T., Adén, D., Meléndez, J., et al. 2011, A&A, 533, A134
Bessell, M. S., & Brett, J. M. 1988, PASP, 100, 1134
Bond, I. A., Abe, F., Dodd, R. J., et al. 2001, MNRAS, 327, 868
Bond, I. A., Udalski, A., & Jaroszyński, M. 2004, ApJL, 606, L155
Bonfils, X., Delfosse, X., Udry, S., et al. 2013, A&A, 549, A109
Borucki, W. J., Koch, D. G., Basri, G., et al. 2011, ApJ, 736, 19
Brown, T. M., Baliber, N., Bianco, F. B., et al. 2013, PASP, 125, 1031
Butler, R. P., Wright, J. T., Marcy, G. W., et al. 2006, ApJ, 646, 505
Cassan, A., Kubas, D., Beaulieu, J.-P., et al. 2012, Natur, 481, 167
Claret, A. 2000, A&A, 363, 1081
Dong, S., Bond, I. A., Gould, A., et al. 2009, ApJ, 698, 1826
Gaudi, B. S. 2012, ARA&A, 50, 411
Gaudi, B. S., Bennett, D. P., Udalski, Al., et al. 2008, Sci, 319, 927
Girardi, L., Bertelli, G., Bressan, A., et al. 2002, A&A, 391, 195
Gould, A., Dong, S., Bennett, D. P., et al. 2010a, ApJ, 710, 1800
Gould, A., Dong, S., Gaudi, B. S., et al. 2010b, ApJ, 720, 1073
Griest, K., & Safizadeh, N. 1998, ApJ, 500, 37
Han, C., & Gould, A. 2003, ApJ, 592, 172
Han, C., Udalski, A., Choi, J.-Y., et al. 2013, ApJL, 762, L28
Holtzman, J. A., Watson, A. M., Baum, W. A., et al. 1998, AJ, 115, 1946
Ida, S., & Lin, D. N. C. 2005, ApJ, 626, 1045
Jaroszyński, M., Skowron, J., Udalski, A., et al. 2010, AcA, 60, 197
Kains, N., Street, R. A., Choi, J.-Y., et al. 2013, A&A, 552, A70
Kennedy, G. M., & Kenyon, S. J. 2008, ApJ, 673, 502
Kennedy, G. M., Kenyon, S. J., & Bromley, B. C. 2006, ApJL, 650, L139
Kervella, P., & Fouqué, P. 2008, A&A, 491, 855
Kervella, P., Thévenin, F., Di Folco, E., & Ségransan, D. 2004, A&A, 426, 297
Lecar, M., Podolak, M., Sasselov, D., & Chiang, E. 2006, ApJ, 640, 1115
Marois, C., Macintosh, B., Barman, T., et al. 2008, Sci, 322, 1348
Mayor, M., & Queloz, D. 1995, Natur, 378, 355

Miyake, N., Sumi, T., Dong, S., et al. 2011, ApJ, 728, 120
Muraki, Y., Han, C., Bennett, D. P., et al. 2011, ApJ, 741, 22
Nataf, D. M., Gould, A., Fouqué, P., et al. 2013, ApJ, 769, 88
Poleski, R., Udalski, A., Dong, S., et al. 2013, ApJ, submitted (arXiv:1307.4084)
Rhie, S. H., Bennett, D. P., Becker, A. C., et al. 2000, ApJ, 533, 378
Sako, T., Sekiguchi, T., Sasaki, M., et al. 2008, ExA, 22, 51
Schechter, P. L., Mateo, M., & Saha, A. 1993, PASP, 105, 1342
Shvartzvald, Y., & Maoz, D. 2012, MNRAS, 419, 3631
Shvartzvald, Y., Maoz, D., Kaspi, S., et al. 2013, MNRAS, submitted (arXiv:1310.0008)
Sumi, T., Abe, F., Bond, I. A., et al. 2003, ApJ, 591, 204

Sumi, T., Bennett, D. P., Bond, I. A., et al. 2010, ApJ, 710, 1641
Sumi, T., Kamiya, K., Bennett, D. P., et al. 2011, Natur, 473, 349
Szymański, M. K., Udalski, A., Soszyński, I., et al. 2011, AcA, 61, 83
Thommes, E. W., Matsumura, S., & Rasio, F. A. 2008, Sci, 321, 814
Tomaney, A. B., & Crotts, A. P. S. 1996, AJ, 112, 2872
Udalski, A. 2003, AcA, 53, 291
Udalski, A., Jaroszyński, M., Paczyński, B., et al. 2005, ApJL, 628, L109
Udalski, A., Szymański, M., Kałużny, J., et al. 1994, AcA, 44, 227
Verde, L., Peiris, H. V., & Spergel, D. N. 2003, ApJS, 148, 195
Yee, J. C., Shvartzvald, Y., Gal-Yam, A., et al. 2012, ApJ, 755, 102